Seasonal Cycles of Along-Track Tropical Cyclone Maximum Intensity

DANIEL M. GILFORD

Department of Earth and Planetary Sciences, Rutgers, The State University of New Jersey, New Brunswick, New Jersey

SUSAN SOLOMON AND KERRY A. EMANUEL

Department of Earth, Atmospheric and Planetary Sciences, Massachusetts Institute of Technology, Cambridge, Massachusetts

(Manuscript received 24 January 2019, in final form 19 April 2019)

ABSTRACT

This study investigates relationships between observed tropical cyclone (TC) maximum intensities and potential intensity (PI) over the seasonal cycle. To directly compare observed and potential intensities, one must account for month-to-month variability in TC tracks and frequencies. Historical TC best track data and reanalysis PI calculations are combined to develop an along-track record of observed maximum and potential intensities for each storm in the satellite-era (1980–2015) across four ocean basins. Overall, observed maximum intensity seasonal cycles agree well with those of along-track PI. An extreme value theory application shows that at least 25 storms must be observed in a given month to have high confidence that the most intense wind speeds of historical TCs follow along-track PI seasonality. In the North Atlantic and Southern Hemisphere regions, there are too few observed storms outside their traditional TC seasons, limiting PI applicability across the seasonal cycle. Small intraseasonal along-track PI variabilities in these regions are driven by TC thermodynamic disequilibrium and sea surface temperatures. Thermodynamic disequilibrium drives seasonal cycles of eastern North Pacific along-track PI and observed maximum intensity, which minimize in August and maximize in June and October. Western North Pacific along-track PI and observed maximum intensity seasonal cycles are relatively flat, and have a local minimum in August because of reduced thermodynamic efficiency, which is linked to anomalously warm near-tropopause outflow temperatures. Powerful ($>65\,\mathrm{m\,s^{-1}}$) western Pacific TCs historically occur in every month except January, due to a combination of tropopause region and SST seasonal influences.

1. Introduction

The development and refinement of potential intensity (PI; Emanuel 1986) has provided the scientific community with a useful theory for understanding how environmental conditions affect upper limits on tropical cyclone (TC) intensity. But the relevance of these theoretical limits for the intensities of real-world tropical cyclones is an active area of research. Relationships between observed and potential intensities have been studied in multiple contexts, including climatology, trends, interannual variability, and "superintensity" (e.g., Emanuel 2000; Persing and Montgomery 2003; Wing et al. 2007; Zeng et al. 2007; Holland and Bruyère 2014; Kossin 2015; Sobel et al. 2016).

A recent study by the authors (Gilford et al. 2017, hereafter GSE17) showed that the seasonal cycle of western North Pacific (WNP) TC PI is relatively flat (seasonally damped) compared to the TC PI seasonalities of the North Atlantic (NA), eastern North Pacific (ENP), and Southern Hemisphere (SH) main development regions. Climatological WNP sea surface temperatures (SSTs) were shown by GSE17 to be perennially warm (>28°C), permitting TC outflow in the WNP to reach the tropopause level in every month of the seasonal cycle. As a result, WNP outflow temperatures follow tropopause seasonality: they are cold in the boreal winter and warm in the boreal summer (Yulaeva et al. 1994), which damps PI seasonality by 30%–40%

Denotes content that is immediately available upon publication as open access.

Supplemental information related to this paper is available at the Journals Online website: https://doi.org/10.1175/MWR-D-19-0021.s1.

Corresponding author: Daniel Gilford, daniel.gilford@rutgers.edu

DOI: 10.1175/MWR-D-19-0021.1

through thermodynamic efficiency (see Table 4.2 and Fig. 4.5 in GSE17). In contrast, SST seasonality dominates the NA TC PI seasonal cycle largely through thermodynamic disequilibrium between the atmosphere and ocean—accounting for nearly three-quarters of the region's seasonal PI range—and to a lesser extent through thermodynamic efficiency. SSTs also exert strong control on the TC PI seasonal cycles in the ENP and SH regions (driving >75% of their seasonal ranges). But how relevant are these PI seasonal cycles for TC intensities observed in the real world?

Emanuel (2000) was the first to empirically show that every observed TC of at least hurricane strength had an equal probability of attaining any lifetime maximum intensity (LMI) up to its along-track climatological-mean potential intensity (i.e., the multidecadal monthly mean PI analyzed at the storm's location). This result implies that changes in climatological PI—such as a long-term trend associated with climate change (Sobel et al. 2016)—should be accompanied by like-changes in observed intensity, and the highest percentiles of observed LMI distributions should consistently scale with PI.

The relationships between observed and potential intensity on interannual time scales were assessed by Wing et al. (2007). Their study showed that there are significant correlations between interannual observed LMIs and potential intensities in the NA and WNP regions over 1950–2005. This result indicated that PI theory is an important predictor for actual tropical cyclone intensities not only climatologically, but also year-upon-year. The goal of our study is to extend the findings and methodologies of Emanuel (2000) and Wing et al. (2007) to the seasonal cycle context, to learn whether there are historically observed manifestations of the intensity seasonal cycles assessed in GSE17.

GSE17 examined PI seasonal cycles averaged over each ocean basin's main development region (MDR; see Table S1 in the online supplemental material), which have been traditionally used in TC studies. Monthly MDR averages in this context implicitly assume that intermonthly excursions in TC tracks are small relative to the intermonthly variability of environmental conditions that influence PI. MDR-averaging further assumes that TCs develop and strengthen within the confines of the defined regions. Observations show, in contrast, that there can be substantial month-to-month differences in tropical cyclone tracks. As tracks migrate, storms will sample different regions of PI (Wing et al. 2007; Kossin and Vimont 2007), which could bias comparisons with actual intensity. Wing et al. (2007), for instance, found that accounting for track variability

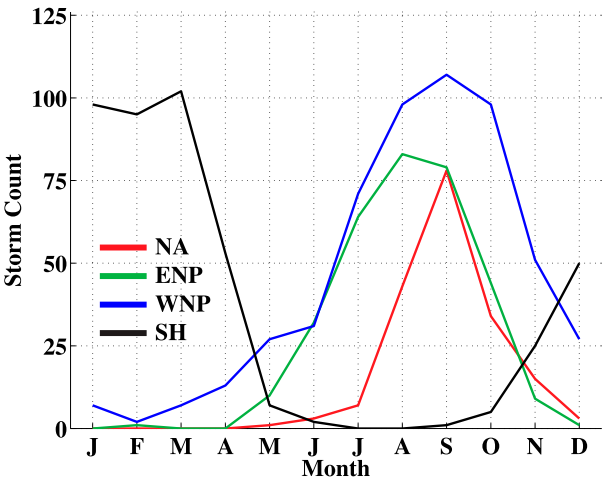

FIG. 1. Seasonal cycles of tropical cyclone frequencies in each TC development region, for storms in the best track data archive that reach a lifetime maximum intensity of more than 32 m s^{-1} (hurricane strength). Each storm's month of occurrence is assigned as the date of its V_{max} (see text). Regions are the North Atlantic (red), eastern North Pacific (green), western North Pacific (blue), and Southern Hemisphere (black).

improved correlations between observed maximum intensities and PI. Kossin et al. (2010) showed that the magnitudes and interpretation of PI trends and variability depend on whether or not track differences are considered. To account for monthly track migrations and compare with observed TC intensities, we develop an along-track dataset of tropical cyclone PI for each storm in the satellite era (1980–2015). The resulting dataset is also compared to MDR-averaged PI from GSE17, to assess the usefulness MDR-averaging in the seasonal cycle context.

Another challenge that must be addressed when investigating maximum intensity seasonal cycles is the well-known seasonality in TC frequencies (e.g., Landsea 1993; NHC 2017, cf. Fig. 1). In this study we use a property of TC along-track observed and potential intensity distributions—namely the uniformity of normalized wind (observed maximum intensity divided by potential intensity) distributions described in Emanuel (2000)—to determine which individual months in each basin have enough historical storms to permit an assessment of PI theory's veracity. Although several studies have corroborated the Emanuel (2000) result that observed TC intensities should scale with PI (Zeng et al. 2007; Swanson 2008), to our knowledge none have yet examined this question in the seasonal cycle context.

The study is organized as follows. Section 2 considers the seasonality of observed TC frequencies and tracks, and details our development of an along-track dataset of tropical cyclone observed and potential intensities. This

section also highlights the importance of normalized wind distributions for comparisons between actual and potential intensities (cf. the appendix). The seasonal cycles of along-track observed and potential intensities in each ocean basin are presented and analyzed in section 3. We summarize study results in section 4 and discuss their implications.

2. Data and methods

a. Best track observations

We use a best track archive (available at ftp://texmex.mit.edu/pub/emanuel/HURR/tracks/) to determine the seasonal cycles of observed TC intensity and develop an along-track potential intensity and observed lifetime maximum intensity dataset (section 2b). Best tracks from the NA and ENP TC regions are from the National Oceanic and Atmospheric Administration's National Hurricane Center/Tropical Prediction Center, and best tracks from the WNP and SH regions are provided by the U.S. Navy's Joint Typhoon Warning Center. For consistency with GSE17, observed TC data over the 1980–2015 period is used for this study. An advantage of limiting our study to the satellite era is that best track quality is improved compared with earlier periods (though there are still sources of uncertainty up to $5\,\mathrm{m\,s^{-1}}$, Torn and Snyder 2012; Landsea and Franklin 2013). We neglect the north Indian region in our study because there are very few (40 total) hurricane-strength storms in the satellite-era record, and they have large track uncertainties (Kossin et al. 2013).

Best track data are reported every 6 h and include latitude–longitude storm center positions and the maximum 1-min averaged sustained winds at 10 m (with a precision of $5\,\mathrm{kt} \approx 2.57\,\mathrm{m\,s^{-1}}$). Storm track observations are occasionally provided at intra 6-hourly periods, but we restrict our analyses to the 6-hourly observations to maintain consistent analysis/interpretation across all storms in the dataset (following Wing et al. 2007). We refer to lifetime maximum intensity (LMI) of each storm as the *first time* a storm achieves its maximum intensity (as some storms may have multiple reported same-valued lifetime maxima; Emanuel 2000). We neglect tropical storms and depressions ($\mathrm{LMI} \leq 32\,\mathrm{m\,s^{-1}}$) in our analyses, focusing instead on hurricane-strength storms for which PI is most relevant.

Investigating the seasonal cycles of paired lifetime maximum and along-track potential intensities requires us to account for seasonal cycles in TC frequencies and tracks. Figure 1 shows the seasonal frequency of TCs of hurricane strength or greater in each region ($\mathrm{LMI} > 32\,\mathrm{m\,s^{-1}}$) and that have a valid "observed maximum intensity" (defined below, see section 2b). The intraseasonal variation of TC frequency is well known, generally showing a peak in a basin's late summer/early fall and a minimum in the winter and spring (e.g., Landsea 1993; Nuemann 1993). Seasonal frequencies are strongly influenced by vertical wind shear, which can limit both the development and strengthening of TCs in the winter months (e.g., Merrill 1988; DeMaria and Kaplan 1994; Aiyyer and Thorncroft 2006; Hendricks et al. 2010; Tippett et al. 2011; Wang et al. 2015).

We implement a statistical framework in the appendix to determine how the seasonality of storm frequencies constrains the ability to observe storms with maximum intensities near the potential intensity. We find that at least 25 storms must be observed in a given month to have 99% confidence that the most intense historically observed wind speeds will fall within 10% of potential intensity (cf. with each month's storm counts in Fig. 1). The months that do not meet this threshold, however, are not disqualified from exhibiting very intense observed storms. We will show in section 3 that months with fewer observations than this "storm count threshold" may historically still have observed intensities very close to potential intensity [the probability of such an event, given a month's frequency, is given by Eq. (A2) in the appendix].

Tropical cyclone tracks and observed maximum locations also show month-to-month variability (Fig 2). WNP TC tracks are more equatorward in the boreal winter months and more poleward in the boreal summer months (e.g., Wang et al. 2015). Figure 3 shows that the monthly average latitudes of each storm's observed maximum intensity (i.e., filled circles in Fig. 2, see section 2b) exhibit this systematic seasonal migration in WNP tracks. ENP tracks follow a similar north–south month-to-month shift (Fig. 3). A seasonal signal in the NA and SH tracks is less obvious, in part because there are far fewer storms in the winter months (cf. Fig. 1), but there are still some seasonal migrations. For instance, storms maximize farther west in the NA basin during the very early or very late months of the hurricane season (e.g., McAdie et al. 2009). Seasonal track migrations imply that storms may sample regions of stronger or weaker PI at different times in the seasonal cycle (Kossin and Vimont 2007; Kossin and Camargo 2009). As implied by the seasonal differences between the average latitudes of along-track TC maximum intensities and the average latitude of each MDR region (Fig. 3), MDR definitions (Table S1, overlaid boxes in Fig. 2) are clearly inadequate to describe the environmental conditions many storms experience during their lifetimes. In the next section, we

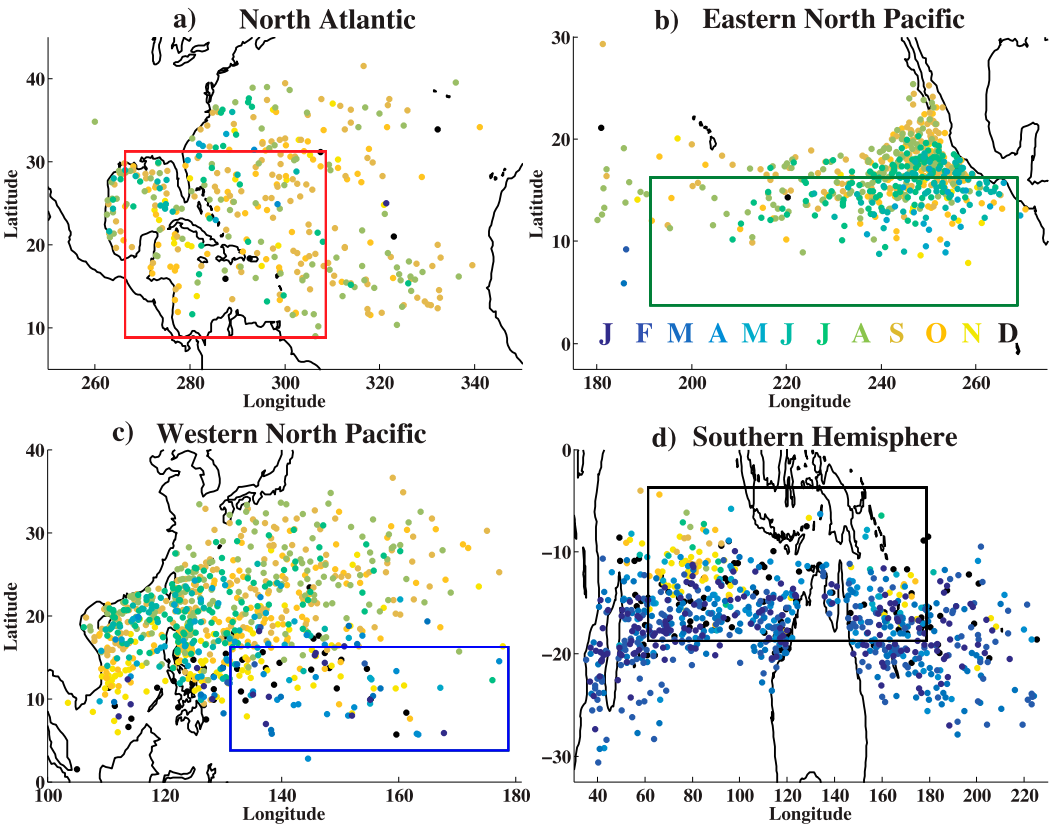

FIG. 2. Locations of each storm's observed maximum intensity (defined in section 2b) from the best track data archive over 1980–2015 for each TC region. Storms are color-coded by the month in which their maximum intensity occurs, with cooler colors representing boreal winter and spring months and warmer colors representing boreal summer and fall months (see legend). Colored boxes indicate the main development regions, as defined in Table S1.

develop an along-track dataset of paired observed and potential intensities designed to address seasonal track differences.

b. *Along-track intensity dataset*

An along-track dataset of tropical cyclone potential intensities is constructed using a climatology calculated with the Bister and Emanuel (2002, hereafter BE02) algorithm and MERRA2 environmental conditions (Gelaro et al. 2017); the full methodology used to produce the PI climatology is described in GSE17. Potential intensities computed with ERA-Interim are similar to those of MERRA2 and have consistent seasonalities (see GSE17's Fig. S1).

The MERRA2 PI climatology—37-yr means (over 1980–2016) at each month/latitude/longitude on a 2.5° × 2.5° grid—is bilinearly interpolated to every TC storm center position in the best track dataset. A cubic spline-fit is used to temporally interpolate the monthly PI climatology to the best track 6-hourly grid, where monthly means are assumed to represent the central day of each month.

We show the time evolution of the along-track observed intensity and potential intensity over the lifetime of Hurricane Jeanne (2004) in Fig. 4 as an example of the temporal and spatial interpolation. Along-track PI values (filled circles) are nearly indistinguishable from the background September-mean PI (contours), indicating that the temporal spline fitting is much less important than the PI spatial variations sampled over the lifetime of Hurricane Jeanne (though these are also small along Hurricane Jeanne's track). As it made landfall in the Caribbean ~175 h before its LMI, Hurricane Jeanne's along-track PI briefly dropped to zero (by definition at landfall). Jeanne next traveled back over open water and looped once, then reached its LMI (at 71% of its concurrent PI) just before a final landfall in Florida in late September.

Climatological potential intensities clearly may differ from the operational potential intensity that a storm experiences (such as the daily potential intensities reported by the Center for Ocean–Land-–Atmosphere studies at http://wxmaps.org/pix/hurpot.html). We chose to use monthly climatologies of PI for three reasons.

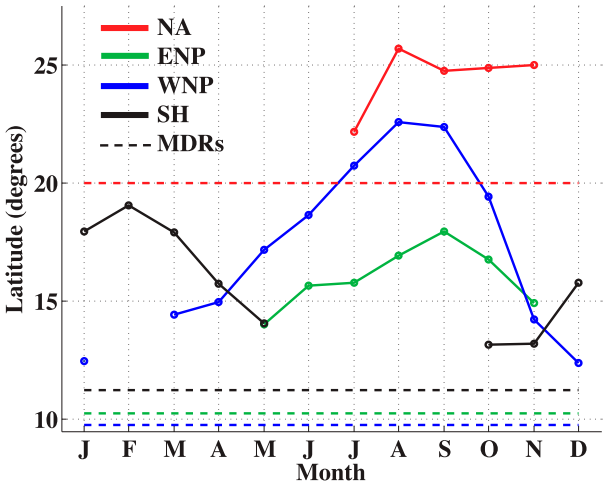

FIG. 3. Seasonal cycles (solid lines) in the average latitudes of each basin's observed maximum intensity (V_{max}, as defined in section 2b); shown for every month with at least five observed storms over 1980–2015. Regions are the North Atlantic (red), eastern North Pacific (green), western North Pacific (blue), and Southern Hemisphere (black). The average latitude of each main development region (which does not vary over the seasonal cycle) is shown for comparison (dashed lines).

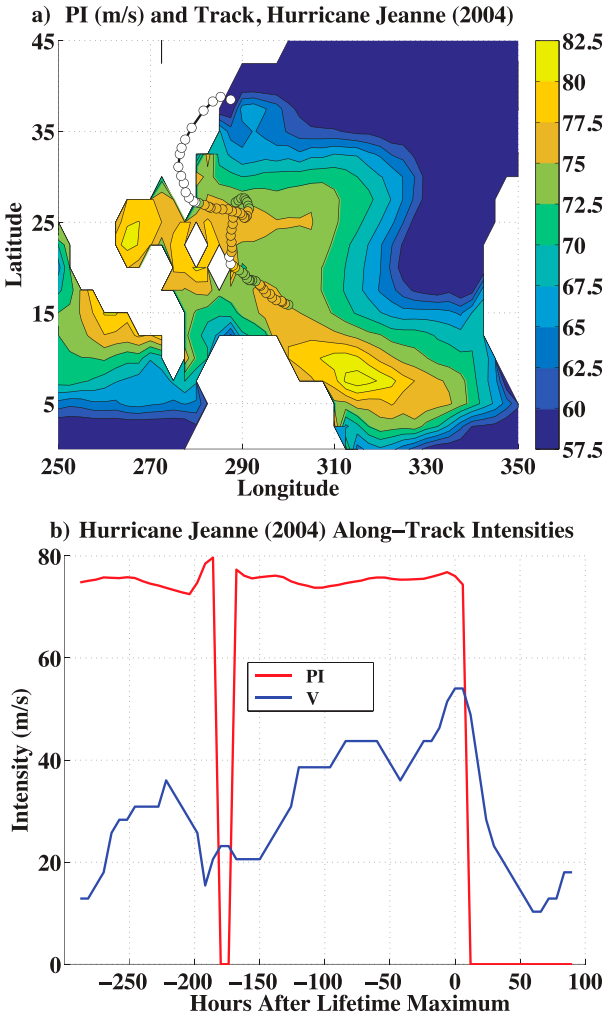

FIG. 4. (a) The North Atlantic climatological potential intensity in September (contoured) and the interpolated along-track potential intensity of Hurricane Jeanne (13–29 Sep 2004, filled circles). Contours are every 2.5 m s^{-1} and saturate at the color bar's extent. White filled circles indicate where the track made landfall ($V_p = 0$). Mismatched intensities between the track and contours illustrate the minor effects of the temporal spline fitting (see text). (b) The along-track observed wind speeds from the best track archive (blue curve) and potential intensity (red curve) of Hurricane Jeanne before and after its lifetime maximum intensity.

First, PI calculations are roughly linear, so that the average PI calculated with a series of environmental conditions is very similar to the PI calculated with an average of those environmental conditions (not shown, see also Swanson 2008). While individual storms may sample variable PI values, long-term averages of along-track PI should be robust if TC track distributions are representative. Second, our goal is to develop an along-track dataset useful for exploring the seasonal cycles of potential intensities that a "typical" TC would experience. For this purpose the operational environments of individual historical storms (which will be sparse in space/time when considered along-track, and will be drawn from a range of internal climate variability) should be less relevant than seasonal climatologies of PI, which provides a good null hypothesis for PI seasonality in a given hurricane season. Finally, along-track values of climatological PI may be directly compared to the MDR averages in GSE17 (e.g., their Fig. 4.1) to determine the influence of intraseasonal track migrations and the usefulness of MDR averages in the seasonal cycle context.

For every storm in the best track dataset, we extract pairs of the along-track climatological potential intensity and a quantity we term the "observed maximum intensity" (V_{max}), which is identical to the LMI when the TC intensity is not limited by landfall or by moving into a region of low PI. Using the criteria of Emanuel (2000), if a storm's LMI occurs over land (where PI = 0, 11.4% of all hurricane-strength storms since 1979) or if a storm's LMI temporarily exceeds PI as it moves from regions of higher to lower PI (4.1% of storms, most often due to passage over cold waters), then we define V_{max} at the location 6 h prior to exceeding PI/making landfall. Storms that 1) had missing data within 24 h of their maximum, 2) were limited by passage over cold water, 3) never emerged over open water during their lifetime, or 4) formed partially over land and had their LMI before emerging over open water, are removed from the dataset. In cases where a storm makes landfall within

24 h of its LMI and LMI > PI (<1% of all storms), V_{max} is retained with the LMI value and location, because it is a relevant maximum intensity for possible coastal impacts. In all other cases V_{max} is either equal to or less than PI. There are 1464 total pairs of V_{max} and PI (at the V_{max} locations) used in our analyses of normalized wind distributions (the appendix) and the seasonal cycles of tropical cyclone maximum intensity (section 3).

We note some limitations that could affect our results. Relevant physical processes may not be appropriately represented in the PI metric (e.g., Bryan and Rotunno 2009; Frisius and Schonemann 2012), for example, the C_k/C_D ratio directly scales the PI magnitude, and has a broad possible range (e.g., Emanuel 2003, and references therein), and operational PI for any given storm could be appreciably higher or lower than the climatological values used to create our dataset (these uncertainties may contribute to a limited subset of the 4.1% of storms that we observe with LMI > PI). Another source of uncertainty may be found in the contributions of TC translation velocity to best track ground-relative wind speeds. Although some studies have shown that accounting for storm translation velocity can improve comparisons between best track and potential intensities (DeMaria and Kaplan 1994; Zeng et al. 2007), the relationship between PI and translation velocity is unclear, in part because ground-relative winds may be more relevant for air–sea interactions than rotational winds (Emanuel 2000). We performed sensitivity analyses and found that when translational velocity is accounted for, best track intensities are reprocessed, and the seasonal cycles of TC maximum intensity are recomputed, our results are qualitatively similar to those presented below (not shown).

c. *Decomposition*

In months where high-percentile observed intensities follow potential intensity seasonality, it is important to quantify how climatological environmental conditions drive along-track potential intensity and bound the most intense real-world storms. We apply a log-additive model to along-track PI seasonal cycles:

$$2 \times \ln(V_p) = \ln\left(\frac{T_S - T_0}{T_0}\right) + \ln(h_o^* - h^*) + C, \qquad (1)$$

where T_s is the sea surface temperature, T_o is the outflow temperature, h_o^* is the saturation moist static energy at the sea surface, and h^* is the saturation moist static energy of the free troposphere. The first decomposed term on the rhs is the contribution to PI from thermodynamic efficiency. The second term on the rhs is the contribution to PI from the disequilibrium between the sea surface and the free troposphere; C is a constant equal to the natural logarithm of the ratio of enthalpy and momentum surface exchange coefficients [fixed at ln(0.9) herein and in GSE17 calculations].

In each region, we decompose the along-track potential intensity in any months that have ≥10 storms. We compute the average of each term in Eq. (1) over the set of all included months and remove this from each month's individual average value to derive seasonal anomalies in along-track PI, thermodynamic efficiency, and thermodynamic disequilibrium. The efficiency term is computed directly with reanalysis SSTs and outflow temperatures derived from the BE02 algorithm. Following GSE17 and Wing et al. (2015), the thermodynamic disequilibrium is evaluated as a residual, and its variability is strongly associated with SSTs when evaluated over a long climatological period (e.g., Emanuel 2007; Wing et al. 2015). Calculating thermodynamic disequilibrium directly produces a qualitatively similar result over the seasonal cycle. PI decomposition is shown for each region in Fig. 5, and discussed further below (section 3).

A particular advantage of along-track decomposition is that it illuminates the seasonal role of outflow temperatures. Recent studies have shown that tropical cyclone outflow temperatures found at or near the tropopause can affect potential intensity (Emanuel et al. 2013; Ramsay 2013; Wang et al. 2014; Wing et al. 2015; Vecchi et al. 2014; Sobel et al. 2016; Walsh et al. 2016; Polvani et al. 2016; GSE17; Ge et al. 2018). Whenever SSTs are seasonally warm they allow deep penetration of TC outflow to the tropopause level, so that temperatures at that level directly influence PI. We note that outflow temperatures are distinct from near-tropopause temperatures when SSTs are relatively cool and the corresponding outflow is not high enough to penetrate the tropopause (i.e., in the months outside the traditional TC season, see discussion in GSE17 and their Fig. 4). During the traditional TC season months in each basin, however, the average outflow level is deep enough that near-tropopause temperatures dictate outflow temperatures. For instance, in the WNP the average outflow level is perennially above the average lapse-rate tropopause height (GSE17, their Fig. 3), and hence the WNP outflow temperature seasonal cycle strongly reflects the seasonality of the tropical lowermost stratosphere.

GSE17 showed the importance of near-tropopause temperature seasonality for PI seasonal cycles. In the months and basins where outflow level lies above the tropopause, the seasonal cycle of near-tropopause temperatures—anomalously warm in the boreal summer and cold in the boreal winter with a seasonal amplitude

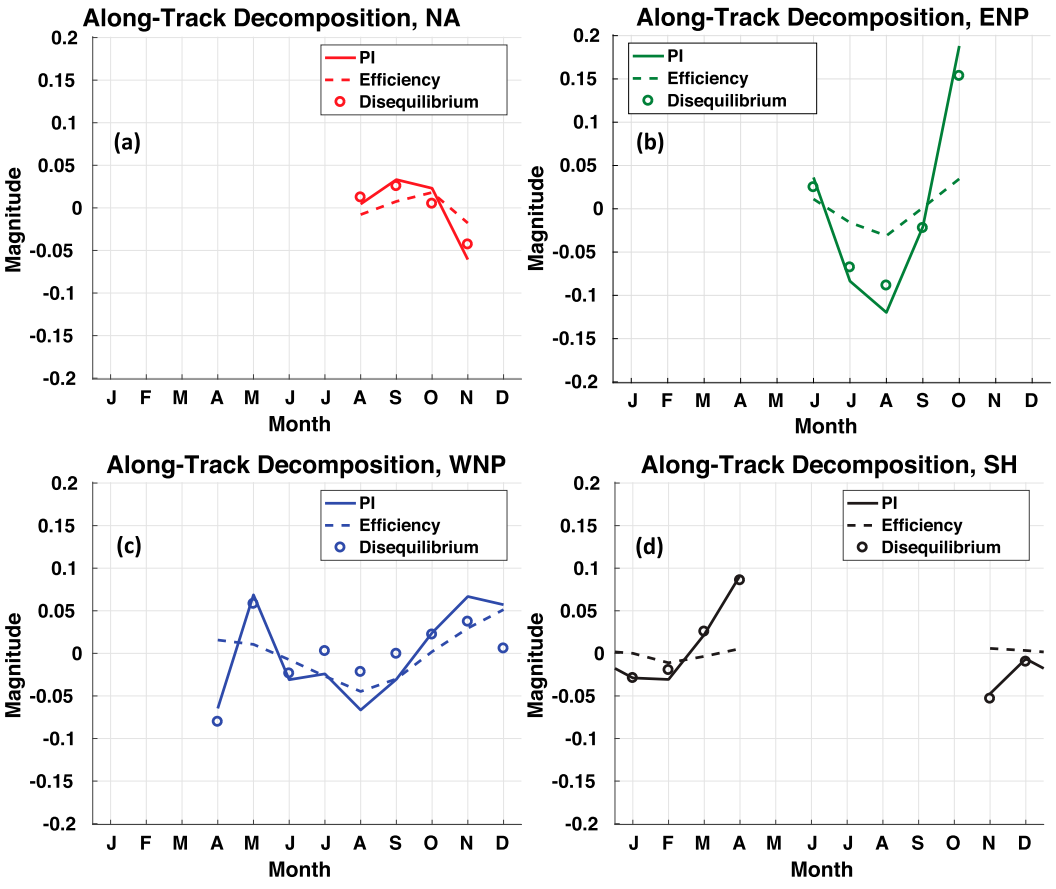

FIG. 5. Along-track seasonal anomalies of 2 times the logarithm of TC PI [solid curves; left-hand-side of Eq. (1)], the logarithm of thermodynamic efficiency [dashed curves; first term on right-hand-side of Eq. (1)], and the logarithm of thermodynamic disequilibrium [circles; second term on right-hand-side of Eq. (1)], for the (a) North Atlantic, (b) eastern North Pacific, (c) western North Pacific, and (d) Southern Hemisphere regions.

of ~8 K (e.g., Yulaeva et al. 1994; Reid 1994; Fueglistaler et al. 2011; Folkins et al. 2006; Chae and Sherwood 2007; Gilford and Solomon 2017)—imprints itself on the seasonal cycle of TC outflow temperatures. Near-tropopause outflow temperatures in turn directly influence thermodynamic efficiency and PI. In the NH regions, when efficiency is seasonally in phase with disequilibrium, the variability in the efficiency term is largely dominated by SST variability (because NH SSTs seasonally maximize in the boreal summer), whereas when efficiency is out of phase with disequilibrium (or the anomalous disequilibrium is close to zero across the seasonal cycle), then outflow temperatures are driving efficiency seasonal variability. In the SH the efficiency phase-relationship is opposite that of the NH: both warm SSTs and cold outflow temperatures increase PI in the austral summer (and likewise combine to decrease SH PI in the austral winter, cf. GSE17, their Fig. 5). Ultimately, determining the seasonality of along-track efficiency with the decomposition method enables us to consider the seasonal influences of near-tropopause outflow temperatures on the upper bounds of real-world TC intensities.

3. Results

The mean of along-track potential intensities (evaluated at each storm's V_{max} location) and the MDR-averaged potential intensities for each TC region are shown in Figs. 6–9. Figures also show the monthly distributions of observed V_{max} with box-and-whisker plots: boxes show the interquartile range (IQR) of V_{max}, whiskers show the full V_{max} range, red ticks show the distribution medians, and outliers ($V_{max} > 1.5 \times$ IQR) are shown as red '+' symbols. If potential intensity theory holds over the seasonal cycle, then the seasonality of the most intense monthly observed intensities (i.e., upper percentiles of the V_{max} distributions) should fall close to mean along-track PI seasonal cycles. For reference, we have included the V_{max} 95th percentiles in each month (P_{95}) as a solid black dot.

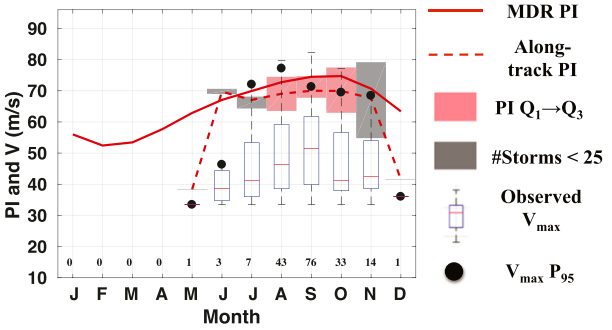

FIG. 6. Seasonal cycles of North Atlantic climatological potential intensity averaged over the main development region (solid curve, Table S1, reproduced from GSE17), and averaged over all climatological potential intensities at the times and locations of the observed tropical cyclone maximum intensities (dashed curve) during the satellite era (1980–2015). Box and whiskers show the monthly distributions of North Atlantic observed maximum intensities (V_{max}). Black dots show the observed distributions' 95th percentiles. Along-track potential and observed intensities are for storms that achieve at least hurricane strength. Numbers below each distribution indicate storm frequency in each month (cf. Fig. 1). Shaded boxes show the interquartile range of each month's along-track PI distribution; boxes are colored if the month's storm frequency is at least 25 storms, and are gray otherwise.

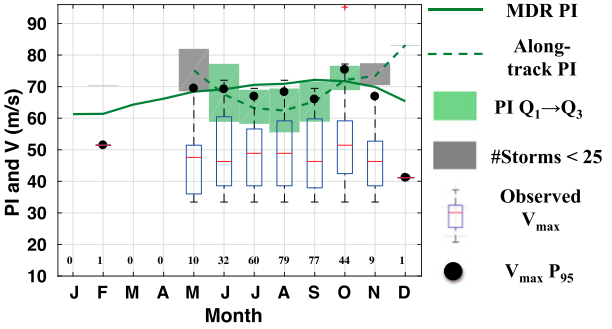

FIG. 7. As in Fig. 6, but for the eastern North Pacific region.

Because no individual V_{max} is tied directly to the mean along-track PI, we illustrate the intramonthly variability of along-track PI with its IQR. Integers above each figure's horizontal axis indicate monthly storm frequencies (reproduced from Fig. 1). Months with at least 25 observed historical storms (i.e., those months that meet the "storm count threshold") have color-shaded along-track PI IQRs, whereas those with less than 25 historical storms have gray-shaded along-track PI IQRs. We present results from each region individually in sections 3a–d.

a. North Atlantic

Maximum intensity seasonal cycles in the NA region (Fig. 6) are marked by a strong dependence on storm frequency (cf. Fig. 1). Only 3 months (August–October) exceed the storm count threshold, and only 6 months have more than a single historical storm that reaches hurricane intensity during 1980–2015. The sharp seasonal gradient in NA frequency is strongly related to seasonal cycles in vertical wind shear (Aiyyer and Thorncroft 2006; Tippett et al. 2011), making historical comparisons between PI and observed maximum intensity useful in only a few months of the year.

From June to November the NA average along-track PI is similar to, but smaller than, NA MDR-averages. In the months where the storm count threshold is met (August–October), the along-track IQR encompasses MDR-average PI, so that MDR-averages are a reasonable estimate for some storms in the region. The seasonal cycle of averaged along-track PI has a very limited range over August–November (2.9 m s^{-1}). Consistent with GSE17, the decomposed disequilibrium term, which is driven by warm boreal summer SSTs on these climatological time scales, closely aligns with the minor changes in decomposed average along-track potential intensity (Fig. 5a). While decomposed efficiency is slightly depressed in August and September when outflow temperatures are warm, NA efficiency overall follows SST seasonality.

Comparing NA observed maximum intensities (V_{max}) to along-track potential intensity, four storms between July and September are landfalling storms that have $V_{max} > V_p$; these storms do not exceed their along-track PI if we account for translation velocity (not shown). Beyond these outliers, along-track PI performs well as a predictor of the high percentiles of V_{max}, acting as a consistent limit on climatological tropical cyclone wind speeds during the NA hurricane season. In both July and November, when the NA storm counts remain small (<15), upper percentiles of historical observed maximum intensity still fall near the along-track PI. Meeting the storm count threshold is therefore not a necessary condition for potential intensity to bound climatological maximum intensities in a given month [although it is less probable when observed storm counts are low, with probability given by Eq. (A2)]. Overall, along-track PI is a reasonable estimate of the most intense historical NA storms over its limited seasonal cycle.

b. Eastern North Pacific

In the ENP region (Fig. 7), like the NA, there are very few storms that occur outside the months of the traditional hurricane season (May–November). But in contrast to the NA region, the average along-track PI seasonal cycle exhibits a starkly different shape than that of the MDR-average PI (which increases steadily from a minima in January to a peak in September). The

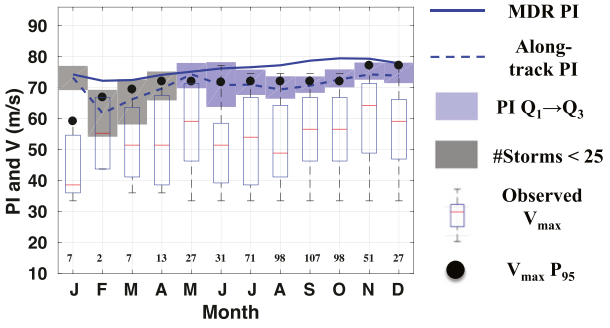

FIG. 8. As in Fig. 6, but for the western North Pacific region.

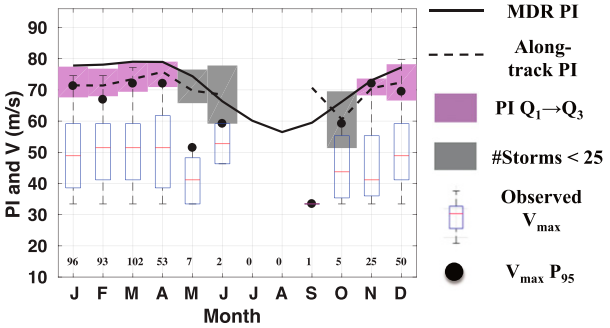

FIG. 9. As in Fig. 6, but for the Southern Hemisphere region.

along-track PI seasonal cycle minimizes in the central months of the hurricane season and maximizes near the edge months of June and October. The contrasting shapes between along-track and MDR-average PI seasonal cycles arise from two key differences. First, the average latitude of boreal summer V_{max} locations is more poleward (Fig. 3) than the extent of the MDR and has colder SSTs (whereas the edge month V_{max} locations are closer to the MDR region, especially in May, June, and November). Second, there is a significant mismatch between ENP V_{max} locations and the MDR, and the discrete monthly V_{max} locations sample a wider variety of environmental conditions than the MDR (Figs. 2 and 3). The difference emphasizes the usefulness of developing an along-track database rather than relying exclusively on MDR-averages.

The ENP region shows the largest average along-track PI seasonal range (12.9 m s^{-1} over May–October) among the basins studied herein (Fig. 5b), with maximum values in the edge months of May and October, and a minimum in the central hurricane season month of August. Consistent with results from GSE17, the seasonality of ENP outflow temperatures is much less influential than seasonal SST variability; a depression in efficiency in the boreal summer months indicates a minor role for seasonally warm outflow (Fig. 5b). The disequilibrium term controls the overall shape of the average along-PI seasonal cycle. This negative disequilibrium anomaly is related to tracks maximizing over colder (higher latitude/farther west) SSTs in the central months of the hurricane season. In June and October average V_{max} locations are closer to the MDR where SSTs are warmer on average than those in the central months of the hurricane season (Fig. 3). This increases the seasonal disequilibrium anomalies in these edge months.

High percentiles of the ENP observed maximum intensity distributions are within the IQRs of along-track PI, and some of the most intense observed storms are found in the edge months of June and October. August is anomalous in that its range spans several m s^{-1} above the along-track PI IQR; the responsible storm, Hurricane Ioke (2006), had a V_{max} of 72 m s^{-1}, but was still below its climatological PI value at its V_{max} location. Intramonthly track variance allows the highest percentile PI values to commonly reach above the mean over all storms, which increases the upper bound on observed intensities. So although each of the 95th percentiles of V_{max} between July and October fall within the IQR of along-track PI, they are all found above the mean over all storms. A key result, therefore, is that although in a typical season the seasonal cycle of PI will tend to limit observed maximum intensities, year-to-year track variability plays an important role in whether a hurricane season's observed maximum intensities will follow the seasonally averaged PI pattern. Track variability permitted the historical storms that became most intense (e.g., the 95th percentile of V_{max}) to sample from potential intensities that were higher than the historical mean of along-track PI. This is a result that would not be apparent from MDR-averaged PI.

A final note on the ENP region is the extreme outlier in October: record-breaking Hurricane Patricia (2015, V_{max} = 94 m s^{-1}). Patricia was the most intense storm (if defined by central pressure, or tied if defined by maximum wind speeds) ever observed in the Western Hemisphere (WMO Weather and Climate Extremes Archive, online at https://wmo.asu.edu). The "extraordinary" storm (Rogers et al. 2017) rapidly intensified under very anomalous local environmental conditions (Huang et al. 2017), and it is therefore unsurprising that climatological PI values are not a viable speed limit for Patricia. Incredibly cold outflow temperatures were observed during its lifetime (Doyle et al. 2017), which may have significantly raised the in situ PI (e.g., Wing et al. 2015). An operational along-track PI dataset would be needed to investigate further. In this work, Patricia demonstrates that although climatological PI is useful for aggregated historical analyses, it is not a

sufficient representation of the intensity limits on any individual storm.

c. Western North Pacific

WNP monthly frequencies exceed the storm count threshold in 8 months (May–December), and 3 of the remaining months (January, March, April) have along-track PI IQRs that encompass the MDR averages. WNP seasonal cycles of along-track PI and MDR-average PI are somewhat similar in shape, but along-track PI has depressions in both the boreal winter and summer months (Fig. 8). While it is not surprising that low-latitude observed maxima in the boreal winter/spring months (often found within the MDR, Figs. 2 and 3) result in similarly high values ($>65\,\mathrm{m\,s^{-1}}$) of average along-track and MDR-average PI, it is remarkable that there are sufficient historical storms to show this feature.

Average WNP along-track PI (Fig. 5c) remains relatively flat (range of $4.9\,\mathrm{m\,s^{-1}}$) over the 9 months where the storm threshold is exceeded (April through December), but there are physical nuances in the month-to-month differences that distinguish this behavior from the other regions. April and May have the largest disequilibrium term values on either side of zero, resulting from a sharp monthly gradient from cooler to warmer SSTs across those months (not shown). In the boreal summer months, however, the anomalous disequilibrium term is close to zero and PI term variability is driven by the efficiency term. The negative efficiency anomalies (June–September, with a local *minimum* in August) are driven by warm along-track outflow temperatures (cf. GSE17, their Fig. 1b), which are found in the tropopause region, and overwhelms the small anomalous disequilibrium term in these months. Although along-track PI seasonality shares a similar midsummer efficiency depression as the MDR-averaged PI, it is overall a deeper minimum. Furthermore, the largest along-track PIs (and also $V_{\max}$, see below) are found in May, November, and December, when outflow temperatures are cooler and anomalous efficiencies are strongly positive relative to the rest of the year.

Distributions of WNP $V_{\max}$ are this study's clearest example of the applicability of potential intensity theory in the seasonal cycle context. The highest $V_{\max}$ percentiles scale consistently with the along-track PI (cf. P_{95} values with PI IQRs) in every month except January. $V_{\max}$ distributions in February, March, and April remain consistent with along-track PI, even though their frequencies fall below the storm count threshold. The historical probability of this occurrence in February (with only two observed storms, and having a maximum normalized intensity of 0.97, see the appendix) was only ~12%, so it is fortunate that the historical applicability of PI in February is demonstrable. The consistent match between WNP PI and $V_{\max}$ is evidence that the environmental conditions that set the seasonal cycles of WNP potential intensity are also relevant for the seasonality of typical real-world Typhoon intensities. Furthermore, historical maximum intensities illustrate that powerful WNP Typhoons ($>65\,\mathrm{m\,s^{-1}}$) can occur (and have occurred) throughout the year, confirming a key conclusion (based on PI theory) made in GSE17. Consistency between $V_{\max}$ and average along-track PI seasonal cycles also implies that warm near-tropopause temperatures act to climatologically limit the intensities of the most powerful historical WNP storms in the boreal summer months. Likewise, cool near-tropopause temperatures act to increase the climatological limits of real-world intensities in the boreal winter months.

d. Southern Hemisphere

The comparison between SH along-track PI seasonal cycles and MDR-averages is qualitatively similar to that in the NA region (Fig. 9). Average along-track PI falls below the MDR-averages in the months where the storm count threshold is exceeded, and storm frequencies strongly limit the applicability of potential intensity in the seasonal cycle context. In the months where there are sufficient SH storms (November through April) there is a very small range ($5.2\,\mathrm{m\,s^{-1}}$) in average along-track PI.

SH along-track PI is slightly increased toward the end of the austral summer in April (consistent with MDR-averages in these months), but beyond this feature intensity seasonality is small. What small monthly variance does exist is strongly coupled to the anomalous disequilibrium term (and thus largely SST variability), and efficiency anomalies are perennially close to zero (Fig. 5d).

The SH $V_{\max}$ distribution in May is a notable example of a month with insufficient observed storms for potential intensity theory to hold. Between November and April, the upper percentiles of the observed maximum intensities are found near along-track PI. Consistent with the other basins, along-track PI is a reasonable approximation of the upper bound on SH observed maximum intensities in each month where the number of observations exceeds the storm count.

4. Discussion and summary

This study combined historical tropical cyclone (TC) best track data with MERRA2 climatologies of TC potential intensity to develop a new along-track dataset of paired TC observed maximum intensities and potential intensities over 1980–2015. The along-track dataset was

used to examine the observed and potential intensity seasonal cycles in the North Atlantic, eastern North Pacific, western North Pacific, and Southern Hemisphere TC development regions. Considering TC potential intensity (PI) along the track of TCs rather than averaging over main development regions (MDRs) accounts for seasonal track differences, which are especially relevant in the Pacific regions. Use of historical TC frequencies, and a simple application of extreme value theory, enabled the identification of months where observed maximum intensities should be consistent with potential intensity theory. Applying a linear decomposition method revealed the roles of thermodynamic efficiency and disequilibrium in the along-track estimates of potential intensity, which upper bound real-world observed tropical cyclone intensities in months where potential intensity theory holds.

The observed maximum intensity of each storm was normalized by its collocated climatological potential intensity. When best-fit linear curves are applied to the empirical cumulative distribution functions of these normalized intensities, the distributions appear uniform, in agreement with previous literature (Emanuel 2000; Zeng et al. 2007; Swanson 2008). A novel contribution of this work is the use of these uniform distributions to constrain the applicability of potential intensity theory. Through extreme value theory, each region's uniform distributions imply that *at least* 25 storms must be observed in a given month to have 99% confidence that at least one of those storms will exhibit a maximum intensity within 10% of its potential intensity. Results show that in each region and month with at least 25 historical storms, the highest percentiles (>90%) of observed maximum intensities are always close to climatological along-track potential intensities. This highlights the value of our statistical methodology, and confirms that the observed seasonal cycle of the most intense TC wind speeds routinely follows the climatological potential intensities dictated by environmental conditions.

Seasonal cycles of along-track observed and potential intensities in the North Atlantic and Southern Hemisphere regions are primarily constrained by TC seasonal frequencies. There is very little month-to-month variability in average along-track potential intensity in these regions (except a small increase in the late boreal winter/early boreal spring months of the Southern Hemisphere), and what variability exists is dominated by SSTs through thermodynamic disequilibrium between the ocean and atmosphere.

Average along-track potential intensities in the eastern North Pacific exhibit a seasonality that maximizes in the edge months of hurricane season (June and October) and minimizes in the central month of the hurricane season (August). This is in contrast with the main development region monthly averages, which predict a steady increase in potential intensity from June to September. The result shows that in some contexts it is important to account for intraseasonal tropical cyclone tracks in potential intensity calculations, as opposed to relying on simple main development region seasonal averages. Potential intensity decomposition shows that the monthly variability is tied to thermodynamic disequilibrium, with SSTs being on average colder (and found at higher latitudes/farther west longitudes) in the central months of the hurricane season, and warmer in the edge months of the season. Eastern Pacific outflow temperatures (which are warm in the boreal summer) play a very minor role in this seasonality through thermodynamic efficiency.

Western North Pacific tropical cyclones have an along-track potential intensity seasonal cycle that is muted throughout the year. In the months with at least 25 historical storms (May–December) the potential intensity range is 4.9 m s^{-1}, and there is a local minimum in August. Decomposition shows that this minimum is associated with warm outflow temperatures found in the tropical tropopause region, which reduces the tropical cyclone efficiency and depresses the potential intensity in the boreal summer months. The limited number of storms in the boreal winter months (January through April) reduces confidence in the precise average along-track potential intensity in those months. However, each month across the seasonal cycle (except January) shows good agreement between along-track PI and the highest percentiles of observed maximum intensities. The tight agreement between observed maximum intensities and along-track potential intensities is strong evidence that the most intense real-world western Pacific tropical cyclones have reduced wind speeds in the boreal summer because of anomalously warm near-tropopause temperatures and have increased wind speeds in the boreal winter because of anomalously cool near-tropopause temperatures.

Several key differences emerge between the MDR-average potential intensities explored in GSE17 and the along-track intensities analyzed herein. Although along-track results are similar in shape to MDR-averaged PI seasonal cycles in the North Atlantic and Southern Hemisphere regions, there are clear distinctions in the Pacific basins, as discussed above. Average along-track potential intensities are weaker than those averaged across the MDRs, primarily because storms consistently reach their maximum intensity at higher latitudes (regions of lower average-PI values) than the MDR bounds. There are also subtleties with physical origins in along-track PI seasonality that are not captured with

MDR-averages (e.g., the highest average-PI values are found in the edge months of the eastern North Pacific hurricane season). Furthermore, the inclusion of track information allows significantly more variance in potential intensity estimates, giving a more complete and complex picture of the seasonal cycles of tropical cyclone maximum intensities. In the absence of predicted or observed tracks, there is still some value in using the GSE17 averages across main development regions as a first approximation of potential intensity limits on real-world tropical cyclone intensity in each ocean basin. Furthermore, there is substantial utility in the MDR-average approach of GSE17 for physical interpretations of intraseasonal PI changes, which are more challenging to study comprehensively along the tracks of observed tropical cyclones.

The methodologies presented here do not explicitly consider the importance of vertical wind shear in maximum intensity seasonality. To the extent that wind shear influences are implicit in historical intraseasonal TC frequencies, they do constrain the applicability of TC PI theory through the statistical storm count threshold in the appendix. Furthermore, although wind shear is an important component in limiting tropical cyclone genesis, in periods of quiescent shear (when a tropical cyclone is more likely to develop) the potential intensity metric in this study should be relevant for both genesis and actual TC intensity (e.g., Nolan and McGauley 2012).

The aggregated historical seasonal cycles of maximum intensity presented here are not directly applicable to any given specific storm. Extremely intense storms such as Hurricane Patricia (2015), in particular, will be subject to in situ environmental conditions that may significantly alter both their operational potential intensities and their actual intensities (Rogers et al. 2017) beyond that predicted by climatologies. Additionally, only very recently are high-resolution measurements of very intense storms yielding observational perspectives of how outflow can impact TC intensity and intensification (Doyle et al. 2017). With future improved TC observations, a fuller picture of the operational seasonal cycles of TC intensity and outflow temperature influences may emerge.

Although potential intensity is frequently invoked for estimates of climate change impacts on tropical cyclone intensity, only a handful of studies have compared observed and potential intensities to date (Emanuel 2000; Wing et al. 2007). Our work has expanded on this exercise in a new context, increasing understanding of the seasonal cycles of tropical cyclone maximum intensities, and developing a framework to determine how many observed storms are needed to have confidence that potential intensity theory should hold. Considering the inherent uncertainties in both historically observed and potential intensities, it is reassuring to see the persistent usefulness of the potential intensity metric.

Acknowledgments. DG, SS, and KE were supported by NSF Grant AGS-1461517. DG was supported by NSF Grant ICER-1663807 and NASA Grant 80NSSC17K0698. DG was also supported by NASA Headquarters under the NASA Earth and Space Science Fellowship Program by Grant NNX14AK83H. The lead author thanks Paul O'Gorman and Daniel Rothenberg for helpful discussions, and three anonymous reviewers whose suggestions improved this manuscript.

APPENDIX

Normalized Wind Distributions

The normalized maximum wind speed of a tropical cyclone (e.g., Emanuel 2000) is

$$\upsilon = \frac{V_{\max}}{V_p}, \tag{A1}$$

where $V_{\max}$ is defined in section 2b, and V_p is the potential intensity at the same location. For example, the normalized wind for Hurricane Jeanne is 54/76 ($\mathrm{m\,s^{-1}}$) = 0.71 (Fig. 4).

Over all storms in each TC development region we find an empirical cumulative distribution function (CDF), $F_e(\upsilon)$, by binning υ values into intervals of 0.01. Consistent with Emanuel (2000), the historical probability distributions of υ appear uniform. Although the physical reasons for this uniformity are not well known, it is found consistently in studies of TC intensity, even when potential intensity is subjected to different physical assumptions (e.g., Zeng et al. 2007; Swanson 2008).

In each basin we find a "best-fit" linear function to $F_e(\upsilon)$ using least squares regression. Then, we assume empirical υ values are drawn from a theoretical uniform distribution—with CDF $F(\upsilon)$—which is bounded below by the best-fit line intercept with cumulative probability = 0.0 and above by 1.0 (i.e., we assume following PI theory that $V_{\max} \leq V_p$). The empirical and theoretical cumulative distributions of each basin's normalized wind speeds are shown in Fig. A1. For comparison we also include best-fit lines, which differ from theoretical cumulative distributions at their υ = 1.0 intercept.

The NA CDF is very close to linear across its range (Fig. A1a). WNP and ENP empirical distributions have probabilities below $F(\upsilon)$ in the central portions of the distribution (Fig. A1b–c). In contrast, empirical υ values

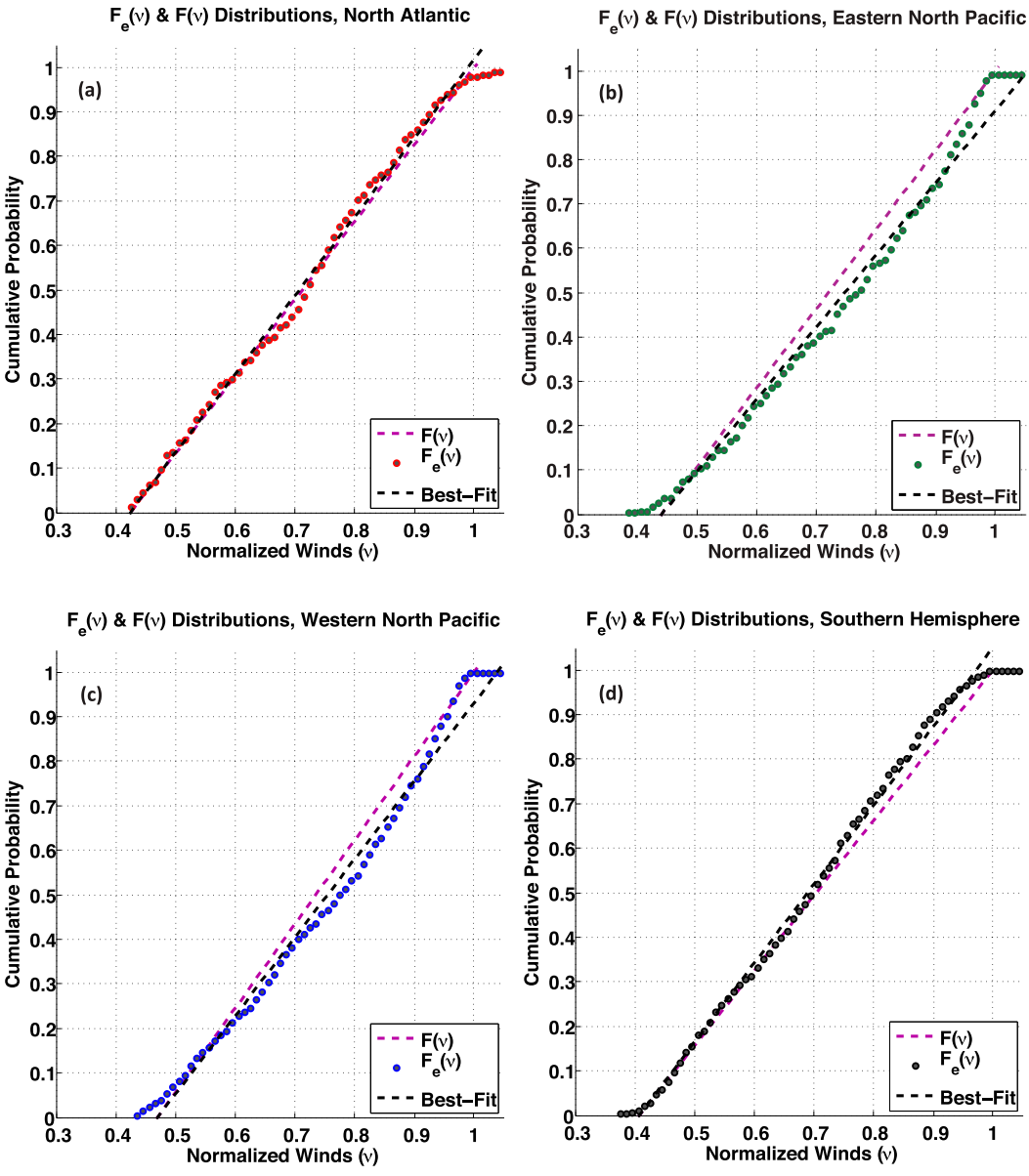

FIG. A1. The empirical (symbols) and theoretical (purple dashed curve) cumulative probability distributions functions of normalized wind speeds [defined by Eq. (A1)] in the (a) North Atlantic, (b) eastern North Pacific, (c) western North Pacific, and (d) Southern Hemisphere regions. Included are the best-fit lines to the empirical distributions (black dashed curves); goodness-of-fit metrics are reported in Table A1.

in the SH are more frequent than $F(v)$ in the central and upper portions of the distribution (Fig. A1d). Differences between basins may arise from variations in data quality. $F_e(v)$ and $F(v)$/best fits are strongly correlated in every region, as computed and shown for each basin in Table A1. These results are similiar to the strongly correlated linear fits ($R^2 \geq 0.98$) to empirical NA and WNP v distributions calculated by Emanuel (2000). While these correlations are a not strict test for uniformity, they are strongly indicative that observed normalized tropical cyclone winds are drawn from a *near*-uniform distribution.

Using $F(v)$, we determine the number of TCs that must be observed to encounter a storm with a v value above a specific threshold. From univariate extreme value theory,

$$P(v > Z) = 1 - [F(Z)]^n, \tag{A2}$$

where Z is some threshold v value, P is the success probability of *at least* one occurrence of $v > Z$, and n is

TABLE A1. Total number of storms that reach at least hurricane intensity in each TC region over 1980–2015, and the Pearson correlation coefficients (squared) between the empirical normalized wind cumulative distributions [$F_e(v)$] and either the best-fit lines (dashed black curves in Fig. A1) or the theoretical normalized wind cumulative distributions [$F(v)$, dashed purple curves in Fig. A1].

Region	No. of TCs	$F(v)$ R^2	Linear Fit R^2
NA	178	0.99	0.99
ENP	313	0.96	0.99
WNP	539	0.97	0.99
SH	434	0.99	0.99

the number of Bernoulli trials performed with probability of occurrence $F(Z)$ (Wilks 1995). With some minor manipulation,

$$n = \frac{\ln(1-P)}{\ln[F(Z)]} \tag{A3}$$

so that the number of Bernoulli trials that must be performed to encounter *at least* one v value larger than Z follows a geometric distribution. In the context of historical TCs, this property shows how many storms drawn from $F(v)$ must be observed to find at least one TC with $v > Z$, with a given confidence level (P). We refer to n as the "storm count threshold."

If we seek to observe at least one hurricane-strength storm with an observed maximum wind speed within 10% of its along-track PI ($v > 0.9$) at a 99% confidence level ($P = 0.99$), then we may apply Eq. (A3) across each region. $F(v = 0.9)$ ranges across the basins between 0.81 (WNP/NA) and 0.83 (SH/ENP), so that ~22–25 storms must be observed. Assuming that $F(v)$ holds over every month, any given month with at least 25 observed storms of hurricane strength is therefore extremely likely have at least one observed storm with V_{max} within 10% of V_p. Referring back to Fig. 1, we now have a constraint on how storm frequency affects the applicability of potential intensity theory, which be applied over every month and region. Note that in principle any given month with fewer than 25 storms may still exhibit one or more V_{max} values close to V_p; the probability of this is given by Eq. (A2), with n being the total number of observed storms in that month. Our choice to seek storms with V_{max} within 10% of PI is arbitrary, but results show (section 3) it is useful minimum, because the highest V_{max} percentiles (≥90%) consistently fall near along-track PI in months with >25 storms.

Note that the assumption of drawing each v from $F(v)$ is not strictly necessary for the application of Eq. (A2). By replacing $F(v)$ with the historical $F_e(v)$ one recovers an ideal historic predictor for the number of storms needed to observe a maximum intensity within some percentage of the climatological potential intensity. But because monthly dependency of v distributions may not historically resemble $F_e(v)$ from the full set of storms in each basin (unknown a priori), we proceed with a storm count threshold from regional $F(v)$ distributions that is grounded, in part, in theory rather than pure empiricism. In all regions except the SH, a theoretical storm count threshold of 25 is conservative, because empirical distributions fall below or align with the theoretical distributions at $v > 0.9$. In the SH, $F_e(v = 0.9)$ is larger than $F(v = 0.9)$, resulting in an empirical estimate of $n \approx 45$. But the seasonal frequency distribution in the SH is sharp enough that only a single month (November) is between the theoretical and empirical estimates for the storm count threshold. The mismatch, by chance, has no bearing on the historical efficacy of potential intensity theory in that month (see Fig. 9).

REFERENCES

Aiyyer, A., and C. D. Thorncroft, 2006: Climatology of vertical wind shear over the tropical Atlantic. *J. Climate*, **19**, 2969–2983, https://doi.org/10.1175/JCLI3685.1.

Bister, M., and K. A. Emanuel, 2002: Low frequency variability of tropical cyclone potential intensity 1. Interannual to interdecadal variability. *J. Geophys. Res.*, **107**, 4801, https://doi.org/10.1029/2001JD000776.

Bryan, G. H., and R. Rotunno, 2009: Evaluation of an analytical model for the maximum intensity of tropical cyclones. *J. Atmos. Sci.*, **66**, 3042–3060, https://doi.org/10.1175/2009JAS3038.1.

Chae, J. H., and S. C. Sherwood, 2007: Annual temperature cycle of the tropical tropopause: A simple model study. *J. Geophys. Res.*, **112**, D19111, https://doi.org/10.1029/2006JD007956.

DeMaria, M., and J. Kaplan, 1994: A Statistical Hurricane Intensity Prediction Scheme (SHIPS) for the Atlantic basin. *Wea. Forecasting*, **9**, 209–220, https://doi.org/10.1175/1520-0434(1994)009<0209:ASHIPS>2.0.CO;2.

Doyle, J. D., and Coauthors, 2017: A view of tropical cyclones from above: The Tropical Cyclone Intensity Experiment. *Bull. Amer. Meteor. Soc.*, **98**, 2113–2134, https://doi.org/10.1175/BAMS-D-16-0055.1.

Emanuel, K. A., 1986: An air–sea interaction theory for tropical cyclones. Part I: Steady-state maintenance. *J. Atmos. Sci.*, **43**, 585–605, https://doi.org/10.1175/1520-0469(1986)043<0585:AASITF>2.0.CO;2.

——, 2000: A statistical analysis of tropical cyclone intensity. *Mon. Wea. Rev.*, **128**, 1139–1152, https://doi.org/10.1175/1520-0493(2000)128<1139:ASAOTC>2.0.CO;2.

——, 2003: Tropical cyclones. *Annu. Rev. Earth Planet. Sci.*, **31**, 75–104, https://doi.org/10.1146/annurev.earth.31.100901.141259.

——, 2007: Environmental factors affecting tropical cyclone power dissipation. *J. Climate*, **20**, 5497–5509, https://doi.org/10.1175/2007JCLI1571.1.

——, S. Solomon, D. Folini, S. Davis, and C. Cagnazzo, 2013: Influence of tropical tropopause layer cooling on Atlantic hurricane activity. *J. Climate*, **26**, 2288–2301, https://doi.org/10.1175/JCLI-D-12-00242.1.

Folkins, I., P. Bernath, C. Boone, G. Lesins, N. Livesey, A. M. Thompson, K. Walker, and J. C. Witte, 2006: Seasonal cycles of O3, CO, and convective outflow at the tropical tropopause. *Geophys. Res. Lett.*, **33**, L16802, https://doi.org/10.1029/2006GL026602.

Frisius, T., and D. Schonemann, 2012: An extended model for the potential intensity of tropical cyclones. *J. Atmos. Sci.*, **69**, 641–661, https://doi.org/10.1175/JAS-D-11-064.1.

Fueglistaler, S., P. H. Haynes, and P. M. Forster, 2011: The annual cycle in lower stratospheric temperatures revisited. *Atmos. Chem. Phys.*, **11**, 3701–3711, https://doi.org/10.5194/acp-11-3701-2011.

Ge, X., D. Shi, and L. Guan, 2018: Monthly variations of tropical cyclone rapid intensification ratio in the western North Pacific. *Atmos. Sci. Lett.*, **19**, e814, https://doi.org/10.1002/asl.814.

Gelaro, R., and Coauthors, 2017: The Modern-Era Retrospective Analysis for Research and Applications, version 2 (MERRA-2). *J. Climate*, **30**, 5419–5454, https://doi.org/10.1175/JCLI-D-16-0758.1.

Gilford, D. M., and S. Solomon, 2017: Radiative effects of stratospheric seasonal cycles in the tropical upper troposphere and lower stratosphere. *J. Climate*, **30**, 2769–2783, https://doi.org/10.1175/JCLI-D-16-0633.1.

——, ——, and K. A. Emanuel, 2017: On the seasonal cycles of tropical cyclone potential intensity. *J. Climate*, **30**, 6085–6096, https://doi.org/10.1175/JCLI-D-16-0827.1.

Hendricks, E. A., M. S. Peng, B. Fu, and T. Li, 2010: Quantifying environmental control on tropical cyclone intensity change. *Mon. Wea. Rev.*, **138**, 3243–3271, https://doi.org/10.1175/2010MWR3185.1.

Holland, G., and C. L. Bruyère, 2014: Recent intense hurricane response to global climate change. *Climate Dyn.*, **42**, 617–627, https://doi.org/10.1007/s00382-013-1713-0.

Huang, H.-C., J. Boucharel, I.-I. Lin, F.-F. Jin, C.-C. Lien, and I.-F. Pun, 2017: Air–sea fluxes for Hurricane Patricia (2015): Comparison with Supertyphoon Haiyan (2013) and under different ENSO conditions. *J. Geophys. Res. Oceans*, **122**, 6076–6089, https://doi.org/10.1002/2017JC012741.

Kossin, J. P., 2015: Validating atmospheric reanalysis data using tropical cyclones as thermometers. *Bull. Amer. Meteor. Soc.*, **96**, 1089–1096, https://doi.org/10.1175/BAMS-D-14-00180.1.

——, and D. J. Vimont, 2007: A more general framework for understanding Atlantic hurricane variability and trends. *Bull. Amer. Meteor. Soc.*, **88**, 1767–1781, https://doi.org/10.1175/BAMS-88-11-1767.

——, and S. J. Camargo, 2009: Hurricane track variability and secular potential intensity trends. *Climatic Change*, **97**, 329–337, https://doi.org/10.1007/s10584-009-9748-2.

——, ——, and M. Sitkowski, 2010: Climate modulation of North Atlantic hurricane tracks. *J. Climate*, **23**, 3057–3076, https://doi.org/10.1175/2010JCLI3497.1.

——, T. L. Olander, and K. R. Knapp, 2013: Trend analysis with a new global record of tropical cyclone intensity. *J. Climate*, **26**, 9960–9976, https://doi.org/10.1175/JCLI-D-13-00262.1.

Landsea, C. W., 1993: A climatology of intense (or major) Atlantic hurricanes. *Mon. Wea. Rev.*, **121**, 1703–1713, https://doi.org/10.1175/1520-0493(1993)121<1703:ACOIMA>2.0.CO;2.

——, and J. L. Franklin, 2013: Atlantic hurricane database uncertainty and presentation of a new database format. *Mon. Wea. Rev.*, **141**, 3576–3592, https://doi.org/10.1175/MWR-D-12-00254.1.

McAdie, C. J., C. W. Landsea, C. J. Neumann, J. E. David, E. S. Blake, and G. R. Hammer, 2009: *Tropical Cyclones of the North Atlantic Ocean 1851–2006.* Historical Climatology Series, Vol. 6 (2), NOAA, 239 pp.

Merrill, R. T., 1988: Environmental influences on hurricane intensification. *J. Atmos. Sci.*, **45**, 1678–1687, https://doi.org/10.1175/1520-0469(1988)045<1678:EIOHI>2.0.CO;2.

NHC, 2017: Tropical cyclone climatology. NOAA/NHC, accessed October 2017, http://www.nhc.noaa.gov/climo/.

Nolan, D., and M. McGauley, 2012: *Tropical Cyclogenesis in Wind Shear: Climatological Relationships and Physical Processes.* Nova Science Publishers, Inc., 36 pp.

Nuemann, C., 1993: Global guide to tropical cyclone forecasting overview. *Global Guide to Tropical Cyclone Forecasting*, Tech. Rep. TCP-31, World Meteorological Organization, 11–27, https://cyclone.wmo.int/pdf/Global-Guide-to-Tropical-Cyclone-Forecasting.pdf.

Persing, J., and M. T. Montgomery, 2003: Hurricane superintensity. *J. Atmos. Sci.*, **60**, 2349–2371, https://doi.org/10.1175/1520-0469(2003)060<2349:HS>2.0.CO;2.

Polvani, L. M., S. J. Camargo, and R. R. Garcia, 2016: The importance of the Montreal Protocol in mitigating the potential intensity of tropical cyclones. *J. Climate*, **29**, 2275–2289, https://doi.org/10.1175/JCLI-D-15-0232.1.

Ramsay, H. A., 2013: The effects of imposed stratospheric cooling on the maximum intensity of tropical cyclones in axisymmetric radiative–convective equilibrium. *J. Climate*, **26**, 9977–9985, https://doi.org/10.1175/JCLI-D-13-00195.1.

Reid, G. C., 1994: Seasonal and interannual temperature variations in the tropical stratosphere. *J. Geophys. Res.*, **99**, 18 923–18 932, https://doi.org/10.1029/94JD01830.

Rogers, R. F., and Coauthors, 2017: Rewriting the tropical record books: The extraordinary intensification of Hurricane Patricia (2015). *Bull. Amer. Meteor. Soc.*, **98**, 2091–2112, https://doi.org/10.1175/BAMS-D-16-0039.1.

Sobel, A. H., S. J. Camargo, T. M. Hall, C.-Y. Lee, M. K. Tippett, and A. A. Wing, 2016: Human influence on tropical cyclone intensity. *Science*, **353**, 242–246, https://doi.org/10.1126/science.aaf6574.

Swanson, K. L., 2008: Nonlocality of Atlantic tropical cyclone intensities. *Geochem. Geophys. Geosyst.*, **9**, Q04V01, https://doi.org/10.1029/2007GC001844.

Tippett, M. K., S. J. Camargo, and A. H. Sobel, 2011: A Poisson regression index for tropical cyclone genesis and the role of large-scale vorticity in genesis. *J. Climate*, **24**, 2335–2357, https://doi.org/10.1175/2010JCLI3811.1.

Torn, R. D., and C. Snyder, 2012: Uncertainty of tropical cyclone best-track information. *Wea. Forecasting*, **27**, 715–729, https://doi.org/10.1175/WAF-D-11-00085.1.

Vecchi, G. A., and Coauthors, 2014: On the seasonal forecasting of regional tropical cyclone activity. *J. Climate*, **27**, 7994–8016, https://doi.org/10.1175/JCLI-D-14-00158.1.

Walsh, K. J. E., and Coauthors, 2016: Tropical cyclones and climate change. *Wiley Interdiscip. Rev.: Climate Change*, **7**, 65–89, https://doi.org/10.1002/wcc.371.

Wang, S., S. J. Camargo, A. H. Sobel, and L. M. Polvani, 2014: Impact of the tropopause temperature on the intensity of tropical cyclones: An idealized study using a mesoscale model. *J. Atmos. Sci.*, **71**, 4333–4348, https://doi.org/10.1175/JAS-D-14-0029.1.

Wang, Y., Y. Rao, Z.-M. Tan, and D. Schönemann, 2015: A statistical analysis of the effects of vertical wind shear on tropical cyclone intensity change over the western North Pacific. *Mon. Wea. Rev.*, **143**, 3434–3453, https://doi.org/10.1175/MWR-D-15-0049.1.

Wilks, D. S., 1995: *Statistical Methods in the Atmospheric Sciences: An Introduction*. International Geophysics Series, Vol. 59, Elsevier, 467 pp.

Wing, A. A., A. H. Sobel, and S. J. Camargo, 2007: Relationship between the potential and actual intensities of tropical cyclones on interannual time scales. *Geophys. Res. Lett.*, **34**, 1–5, https://doi.org/10.1029/2006GL028581.

——, K. Emanuel, and S. Solomon, 2015: On the factors affecting trends and variability in tropical cyclone potential intensity. *Geophys. Res. Lett.*, **42**, 8669–8677, https://doi.org/10.1002/2015GL066145.

Yulaeva, E., J. R. Holton, and J. M. Wallace, 1994: On the cause of the annual cycle in tropical lower-stratospheric temperatures. *J. Atmos. Sci.*, **51**, 169–174, https://doi.org/10.1175/1520-0469(1994)051<0169:OTCOTA>2.0.CO;2.

Zeng, Z., Y. Wang, and C.-C. Wu, 2007: Environmental dynamical control of tropical cyclone intensity—An observational study. *Mon. Wea. Rev.*, **135**, 38–59, https://doi.org/10.1175/MWR3278.1.